

# Spectroscopy of Mg atoms solvated in helium nanodroplets

J. Reho, U. Merker, M. R. Radcliff, K. K. Lehmann, and G. Scoles

*Department of Chemistry, Princeton University, Princeton, New Jersey 08544*

(Received 17 December 1999; accepted 17 February 2000)

We have measured the laser-induced fluorescence excitation spectra of the  $3^1P_1^0 \leftarrow 3^1S_0$  transition of Mg atoms solvated in helium nanodroplets. The observed blue shifts and line broadenings mirror the shifts and broadenings observed in studies of Mg atoms solvated in bulk liquid helium. This similarity allows us to conclude that Mg atoms reside in the interior of the helium droplet. The  $3^1P_1^0 \leftarrow 3^1S_0$  transition shows a splitting which we attribute to a quadrupolelike deformation of the cavity which forms around the solute atom after excitation. Temporal evolution of the fluorescence from the solvated  $3^1P_1^0$  Mg yields a longer lifetime ( $2.39 \pm 0.05$  ns) than found in vacuum ( $1.99 \pm 0.08$  ns). This difference can be accounted for quantitatively by evaluation of the anisotropic distribution of the helium density in the neighborhood of the excited Mg atom. The question of solvation vs surface location for the guest atoms is also discussed in light of the model of Ancilotto *et al.* [F. Ancilotto, P. B. Lerner, and M. W. Cole, *J. Low Temp. Phys.* **101**, 1123 (1995)], of existing metal atom–helium potential energy functions, and of our own calculations for the MgHe and CaHe ground states. While the Ancilotto model successfully predicts solvation (or lack of it) if the solvation parameter of the guest atom is not too near the threshold of 1.9, the present knowledge of the interatomic potentials is not precise enough to test the model in the neighborhood of the critical value. © 2000 American Institute of Physics. [S0021-9606(00)01018-7]

## I. INTRODUCTION

The use of atoms solvated in or attached to helium nanodroplets has allowed for the investigation of the properties of both the dopant atoms themselves and their ultracold droplet hosts.<sup>1,2</sup> One central question for any given probe atom is whether it resides in the interior or on the surface of the droplet. Earlier investigations in our laboratory have shown that alkali atoms<sup>3</sup> and their oligomers<sup>4,5</sup> reside as surface species on helium droplets, corroborating previous theoretical predictions.<sup>6,7</sup> Recently, the same has been observed to be the case for Ca,<sup>8</sup> Sr,<sup>8</sup> and Ba<sup>9</sup> atoms. However, other atomic dopants such as Eu<sup>10</sup> and Ag<sup>11</sup> have been observed to reside inside large helium droplets.

Because this is a central issue in this type of spectroscopy, several theoretical investigations have been carried out in the attempt to understand and thus predict the energetics of solvation of the probe atoms.<sup>1</sup> Using the dopant–He pair potential, Ancilotto *et al.*<sup>12</sup> have devised a relatively simple model which treats the question of solvation for a given dopant. This model proposes that solvation can be predicted by means of a dimensionless parameter  $\lambda$  which compares the gain in energy due to the interaction between the dopant atom and the helium solvent against the cost in energy from creating a cavity within the liquid helium. Formally,

$$\lambda \equiv 2^{-1/6} \sigma^{-1} \rho \epsilon r_e,$$

where  $\sigma$  is the surface tension of the liquid ( $0.179 \text{ cm}^{-1} \text{ \AA}^2$ ),<sup>13</sup>  $\rho$  is the number density ( $0.022 \text{ \AA}^{-3}$ ),<sup>13</sup> and  $\epsilon$  and  $r_e$  are the well depth and equilibrium bond distance of the relevant solute–solvent pair potential, respectively.

Based upon He density functional calculations, Ancilotto *et al.* predict that atoms with values of  $\lambda$  less than 1.9 reside

on the surface, while dopants with  $\lambda$  values greater than 1.9 are expected to be solvated. The model is successful in predicting that alkali atoms ( $\lambda \approx 0.7$ ) (Ref. 12) are located on the surface and in predicting the solvation of Ag ( $\lambda \approx 5$ ) (Ref. 14) and SF<sub>6</sub> ( $\lambda \approx 19$ ).<sup>12</sup> A sensitive test of this model, however, is best carried out with dopants yielding  $\lambda$  values closer to 1.9. The present study involving Mg atoms gives us such an opportunity as the calculated  $\lambda$  value of Mg is close to the solvation threshold.

We have obtained both frequency- and time-resolved spectra of Mg atoms seeded in helium nanodroplets. Our experimental apparatus and laser system are described in Sec. II below. The experimental results obtained in our frequency-resolved studies are described in Sec. III. These results are complemented by our theoretical investigations of the MgHe and CaHe ( $X$ )  $1^1\Sigma$  potential energy surfaces (Sec. IV) which, in combination with helium density functional calculations (Sec. V), have allowed for a better understanding of this problem. Measurements of the fluorescence decay of gas-phase Mg atoms and Mg atoms solvated in He droplets, which yield differing lifetimes, are presented in Sec. V. This result can be quantitatively explained using a density functional-based model.

## II. EXPERIMENT

The apparatus used in the production of doped helium nanodroplets has been reported previously in detail.<sup>3,15</sup> A schematic of it is shown in Fig. 1. Here we offer only an overview of the production of Mg-doped helium droplets, describing in detail only the Mg oven and cell which received a cursory treatment in Ref. 15.

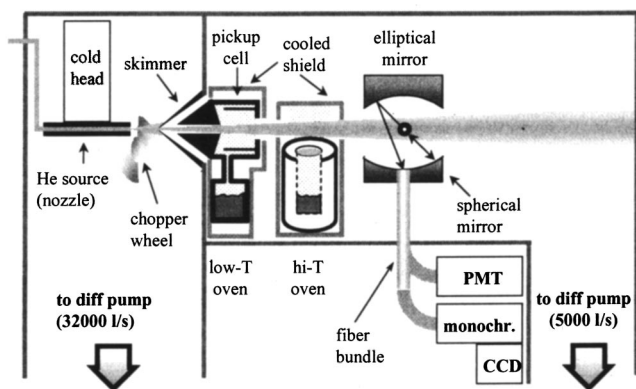


FIG. 1. Experimental apparatus used for studying helium nanodroplets containing guest atoms.

The production of large He nanodroplets ( $\langle N \rangle \sim 10^3 - 10^4$ ) is done by allowing a free jet expansion of He gas with a stagnation pressure of 2.5 MPa through a 20  $\mu\text{m}$  diameter nozzle held at a temperature of 20–16 K. After collimation by a 400  $\mu\text{m}$  skimmer, the droplets are doped with Mg atoms from our Mg pick-up source. This Mg pick-up source is composed of a cylindrical cell of 7 mm inner diameter and 25 mm in length. The cell is positioned in the beam line and is connected via a short tube to an oven reservoir in which solid Mg is contained. Both the oven and cell are resistively heated (Watlow 50 W heaters) to generate typical vapor pressures between  $10^{-2} - 10^{-1}$  Pa of Mg in the oven and cell. The cell is kept 100 K hotter than the oven to avoid condensation. Oven temperatures up to 700 K are reached in this source. The unit is connected to a water-cooled Cu block to prevent damage from excessive heat.

Nearly 22 cm from the nozzle, the doped helium nanodroplets encounter the laser light probe. The laser beam intersects the molecular beam perpendicularly at the center of a two-mirror laser-induced fluorescence detector. In the collection of time-resolved spectra one of these mirrors is omitted.<sup>16</sup> The laser-induced fluorescence is focused onto a multimode, incoherent fiber bundle (Edmund Scientific H38956) and is brought to a microchannel plate detector (Hamamatsu R2807U-07). In the collection of frequency-resolved spectra with pulsed lasers, this signal is amplified and then processed by a boxcar integrator with a gate width of 7 ns. The exciting laser beam itself, after crossing the molecular beam, is detected by a photomultiplier tube or a fast photodiode and is processed by another boxcar integrator.

Reversed time-correlated single photon counting is used in the collection of our time-resolved spectra. Our photon counting apparatus is described in detail elsewhere.<sup>16</sup> Summarily, the signal arising from the microchannel plate detector and the signal arising from the correlated laser pulse impinging on a fast photodiode are processed by constant fraction discriminators and then by a time-to-amplitude converter (TAC). The output of the TAC is processed by a multichannel analyzer which contains 8192 channels. The multichannel analyzer is set to cover a 320 ns region of time, and

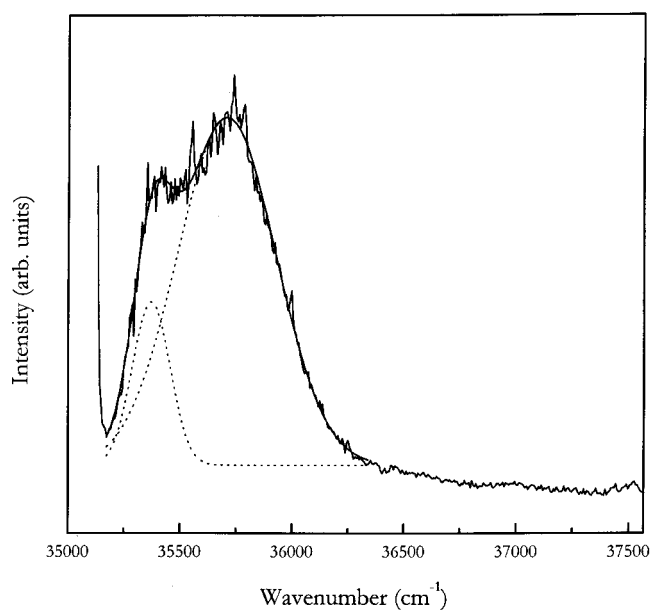


FIG. 2. The  $3\ ^1P_1^0 \leftarrow 3\ ^1S_0$  transition of Mg atoms solvated in helium nanodroplets. The best fit to the data by two Gaussian line shapes is also shown.

the photon counting instrument itself has a time resolution<sup>17</sup> of 50 ps.

The laser light used in the frequency-resolved studies is generated in the Center for Ultrafast Laser Applications (CULA) located in the Department of Chemistry of Princeton University in a facility just above our laboratory. This system, described in detail previously,<sup>15</sup> centers on a Ti:sapphire laser (Spectra Physics Tsunami) mode-locked at 80 MHz which is regeneratively amplified by means of a Spectra-Physics Spitfire amplifier and then further enhanced by a double-pass unit located within the latter. The doubled output of the Spitfire pumps a TOPAS optical parametric amplifier, the final output of which is continuously tunable from 235 to 800 nm. Typical pulse energies of 5  $\mu\text{J}$  per pulse (i.e., 5 mW average power) are measured at the entrance to our molecular beam apparatus. The spectral width of the laser pulses was determined by scanning the  $3\ ^1P_1^0 \leftarrow 3\ ^1S_0$  gas-phase transition of atomic Mg, and in the present study has been measured to have a FWHM of 25  $\text{cm}^{-1}$ . The frequency of the TOPAS amplifier is calibrated against the spectral lines of an Fe–Ne hollow cathode lamp,<sup>18</sup> making use of the optogalvanic effect.

Our time-resolved studies were done by doubling (using a  $\beta$ -barium borate crystal) the output of a Coherent 700 dye laser equipped with a 7220 cavity dumper running Rhodamine 6G dye. This dye laser is pumped by a Coherent Antares mode-locked, doubled YAG laser. The repetition rate of the dye laser is altered from its nominal 76 MHz rate to 3.8 MHz by use of the cavity dumper. Typical average output powers of the doubled light were 1.8–2.5 mW.

### III. EXCITATION SPECTRA

The spectrum of the  $3\ ^1P_1^0 \leftarrow 3\ ^1S_0$  transition of Mg atoms attached to helium nanodroplets is shown in Fig. 2. The absorption is broad (FWHM of 660  $\text{cm}^{-1}$ ) and is strongly

TABLE I. Parameters of the Gaussians representing the best fit to the spectrum of Mg atoms solvated in helium droplets shown in Fig. 1. The errors reported are based upon the fit to the data.

Gaussian	Center (cm <sup>-1</sup> )	FWHM (cm <sup>-1</sup> )	Relative area (%)
I	35 358±2	162±6	13±1
II	35 693±3	460±6	87±1

blue-shifted from its position in the gas-phase. The line shape of the spectrum is well fitted by two Gaussians which are also shown in Fig. 2 as dashed lines. The best fit parameters are reported in Table I. As reported in the table, the central positions of the two spectral components differ by 335 cm<sup>-1</sup> and correspond to shifts of 307 cm<sup>-1</sup> and 642 cm<sup>-1</sup> from the gas-phase value<sup>19</sup> of 35 051 cm<sup>-1</sup>.

In a recent study, Moriwaki *et al.* have measured this same  $3^1P_1^0 \leftarrow 3^1S_0$  transition for Mg atoms solvated in bulk liquid helium.<sup>20</sup> The comparison of their spectrum with ours is shown in Fig. 3, in which the heavier line corresponds to Mg in the bulk liquid and the thinner to Mg attached to helium droplets. Except for the appearance of the gas-phase  $3^1P_1^0 \leftarrow 3^1S_0$  Mg line, which appears in our spectrum due to the presence of gas-phase Mg in our chamber, the overlap of the two spectra is remarkable. We contrast this similarity with the spectra of alkali atoms attached to helium droplets, which are known to reside above a dimplelike well on the surface of the droplet. These alkali atoms show only small shifts from their gas-phase frequency positions<sup>3</sup> in comparison with the case of alkali atom solvation in bulk liquid helium.<sup>21</sup> Bearing this in mind, the large shift of the Mg spectrum from the gas-phase position and its quantitative overlap with that obtained in the case of solvation in the bulk liquid clearly demonstrate the interior position of this atom.

The doubly-shaped profiles of the  $D_2 (n^2 P_{3/2} \leftarrow n^2 S_{1/2})$  lines of Rb ( $n=5$ ) and Cs ( $n=6$ ) atoms in bulk liquid helium as observed by Kinoshita *et al.*<sup>21</sup> are seen to be similar to that observed above for Mg. Kinoshita *et al.* reach a qualitative understanding of this profile through a deformed bubble model in which oscillatory quadrupole deformations of the cavity surrounding the alkali atom dopant split the degenerate atomic state. Likewise, we have observed similar spectral profiles by exciting the  $3^2D \leftarrow 3^2P$  transition of Al atoms solvated in helium droplets.<sup>15</sup> Here too, the doubly-shaped profiles, which are not attributable to any atomic splitting in the Al itself, have been attributed to a quadrupolelike deformation of the cavity surrounding the solvated atom.<sup>15</sup> As the excited Mg atom exhibits nonspherical valence electron distribution similar to the ( $nP$ ) alkali and Al dopants, it is reasonable to postulate that similar quadrupolelike deformations of the helium cavity produce the characteristic spectral splitting for Mg as well.

#### IV. THE Ca/Mg-He POTENTIAL ENERGY SURFACES AND THE "IN VS OUT" QUESTION

The spectra recorded for the  $1^1P_1^0 \leftarrow 1^1S_0$  transitions of Ca, Sr, and Ba attached to large He droplets by Stienkemeier and co-workers show only about one-half of the broadening and approximately one-third of the shift obtained for the same transitions in bulk liquid helium.<sup>8,9</sup> The smaller blue-shift, and to a lesser extent the decrease in spectral width, are presented by the authors of Ref. 8 as primary evidence for a surface location of Ca and Sr on the droplet. While the authors point out that not all experimental and theoretical evidence points uniformly to a surface location of the Ca or Sr dopants, the surface location in the case of Ba is reported as more clear-cut.<sup>9</sup>

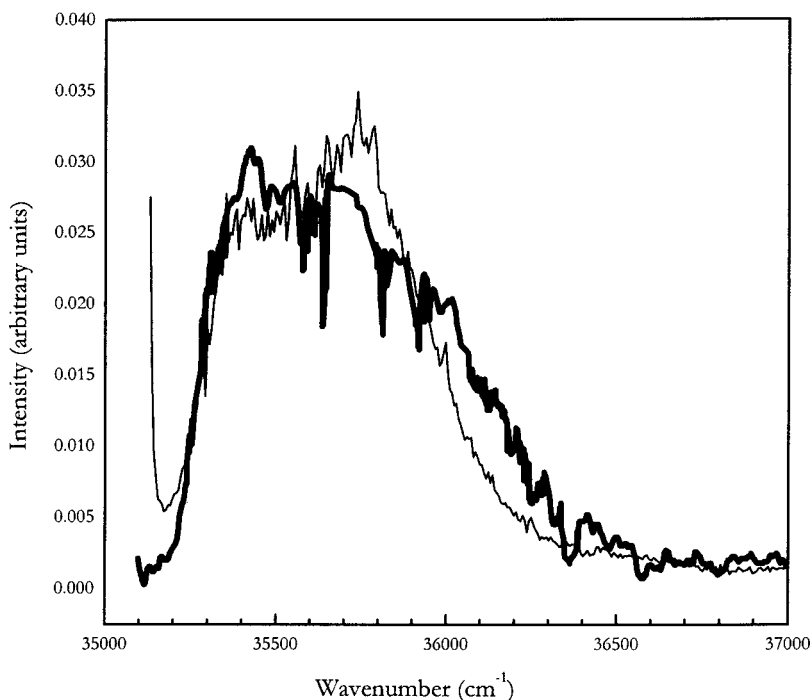


FIG. 3. Comparison of the  $3^1P_1^0 \leftarrow 3^1S_0$  transition of Mg atoms picked up by He nanodroplets (thin line) and solvated in bulk liquid helium (thick line).

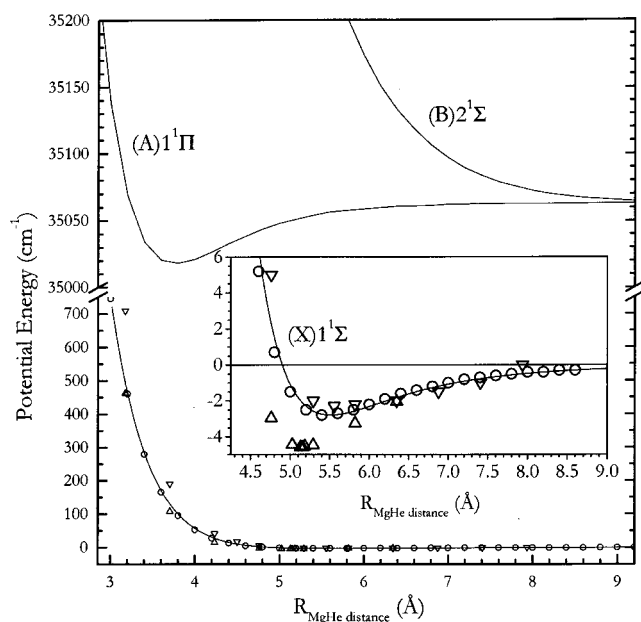


FIG. 4. The  $(X)1^1\Sigma$  potential energy surfaces of MgHe as calculated by the MP2 (circles) (Ref. 30), SCF/CI (downward triangles) (Ref. 21), MP4 (upward triangles) (Ref. 28), and HFD (solid line) (Ref. 24) methods. Also shown are the first two excited states of singlet MgHe ((A) $1^1\Pi$  and (B) $1^1\Sigma$ ) as calculated using MP2.

As mentioned in the Introduction, predictions of solvation based upon the model of Ancilotto *et al.* depend upon both the well depth and the equilibrium internuclear distance of the given dopant-He pair potential. For instance, use of the CaHe  $(X)1^1\Sigma$  surface of Czuchaj *et al.*<sup>22</sup> yields a  $\lambda$  value of 2.1 for Ca, predictive of solvation within the Ancilotto model. The CaHe  $(X)1^1\Sigma$  surface of Kleinekathöfer<sup>23</sup> (for which  $\lambda=5.5$ ) predicts Ca to be solvated even more strongly. However, experimental observation has shown these atoms to be resident on the surface of helium droplets.<sup>8</sup> We have therefore evaluated the potential energy surfaces of the atom combinations which serve as input for the Ancilotto model. In so doing, we have produced the  $(X)1^1\Sigma$  surfaces of MgHe and CaHe using the Hartree-Fock damped dispersion ansatz<sup>24</sup> a widely used semiempirical method which has been found to be quite accurate for first and second row atom combinations.<sup>24,25</sup>

The semiempirical HFD method describes the potential energy surface in terms of two components. One component ( $\Delta E_{\text{SCF}}$ ) is calculated at the Hartree-Fock self-consistent field level of theory. The other contribution ( $\Delta E_{\text{corr}}$ ), which accounts for dispersion interactions, is accounted for by the standard damped multipolar expansion. The  $C_n$  coefficients used in the calculation of the  $\Delta E_{\text{corr}}$  component of the  $(X)1^1\Sigma$  state of MgHe were taken from values reported by Standard and Certain<sup>26</sup> while the Hartree-Fock energy used as  $\Delta E_{\text{SCF}}$  is calculated in the 6-311+G(3df) basis using the GAUSSIAN 94 suite of programs,<sup>27</sup> correcting for the basis set superposition error (BSSE) at each point.<sup>27</sup>

Figure 4 illustrates the MgHe  $(X)1^1\Sigma$  surfaces calculated by Funk *et al.*,<sup>28</sup> Czuchaj *et al.*,<sup>29</sup> Hui and Takami,<sup>30</sup> and in our group. The surface of Funk *et al.* is calculated using fourth-order Møller-Plesset perturbation theory, and is

TABLE II. Comparison of the well depth ( $\epsilon$ ) and internuclear distance ( $r_{\text{min}}$ ) of the  $1^2\Sigma$  surfaces of MgHe as calculated by the ATT (Ref. 23), MF4 (Ref. 28), SCF/CI (Ref. 29), RHF/MP2 (Ref. 30), and HFD methods (Ref. 24) and of CaHe as calculated by the ATT (Ref. 23), SCF/CI (Ref. 22), and the HFD method (Ref. 24). In the third column the corresponding values obtained for the parameter  $\lambda$  of Ancilotto *et al.* (Ref. 12) are reported.

$(X)1^1\Sigma$ Surface of MgHe	$\epsilon$ ( $\text{cm}^{-1}$ )	$r_e$ ( $\text{\AA}$ )	$\lambda$
MP2	2.8	5.4	1.6
MP4	4.6	5.2	2.5
SCF/CI	2.3	5.6	1.4
ATT	7.7	4.7	3.8
HFD	2.8	5.4	1.6
$(X)1^1\Sigma$ Surface of CaHe			
SCF/CI	2.9	7.4	2.1
ATT	10.3	5.1	5.5
HFD	2.03	6.6	1.4

referred to as the MP4 surface in the figure and hereafter. This MP4 surface uses an augmented Gaussian basis built on that of Huzinaga *et al.*<sup>31</sup> for Mg, and employs a  $[10s3p2d1f/5s3p2d1f]$  Gaussian basis inclusive of the 10s set of van Duijneveldt<sup>32</sup> for He. The surface of Czuchaj and co-workers represents a pseudopotential SCF/CI calculation and is hereafter referred to as SCF/CI. The surface of Hui and Takami was calculated using second-order Møller-Plesset perturbation theory and is labeled as the MP2 surface. This surface employs the cc-pVQZ((7s3p2d1f)/[4s3p2d1f]) Gaussian-type orbital basis set of Woon and Dunning<sup>33</sup> for the He atom and a 6-311+G(3df,3pd) basis<sup>34,35</sup> for Mg. We also consider the MgHe  $(X)1^1\Sigma$  surface of Kleinekathöfer,<sup>23</sup> which has been calculated using an adaptation of the Tang and Toennies semiempirical model,<sup>36</sup> and is thus referred to as the ATT surface.

Well depth  $\epsilon$  and equilibrium internuclear distance  $r_e$  for all of these MgHe surfaces are reported in Table II. It is seen from Fig. 4 and Table II that the MgHe  $(X)1^1\Sigma$  HFD potential, plotted as a solid line, shows good agreement with the MP2 and the SCF/CI surfaces but substantially deviates from the ATT and MP4 potentials. The SCF/CI surface, generated from pseudopotential SCF/CI calculations, seems to somewhat underestimate the depth of the potential well and proportionally overestimate the size of the zero of the potential as higher repulsion is predicted than in the case of the others. As shown in Table II, the Ancilotto solvation parameter,  $\lambda$ , varies from 1.4 to 3.8 for these potential surfaces. The MP4 and ATT potential correctly predict solvation while the other three potentials yield a  $\lambda$  value which slightly favors a surface location.

The  $(X)1^1\Sigma$  surface of CaHe has also been calculated by the HFD method. The uncorrelated component ( $\Delta E_{\text{SCF}}$ ) of this surface has been calculated using the 6-311G(2df) basis<sup>37</sup> for Ca and the 6-311+G(3df) basis for He. Correlations are introduced as described above, again employing the pertinent  $C_n$  coefficients taken from Standard and Certain.<sup>26</sup> This CaHe  $(X)1^1\Sigma$  HFD surface, shown in Fig. 5, has a well depth  $\epsilon$  of 1.3  $\text{cm}^{-1}$  and an  $r_{\text{min}}$  value of 6.9  $\text{\AA}$ ,

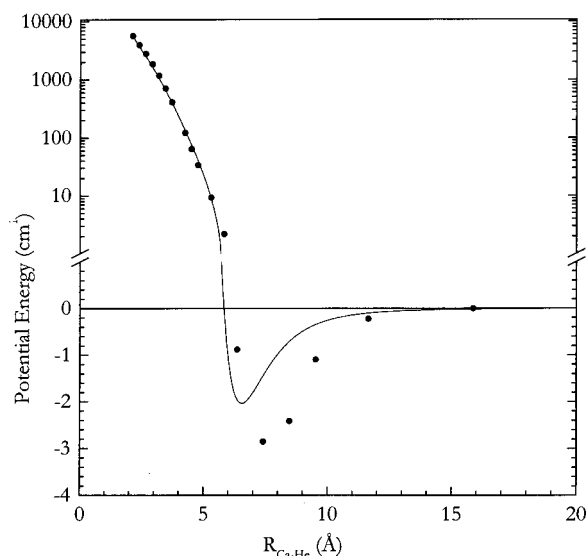


FIG. 5. The  $(X)1^1\Sigma$  potential energy surface of CaHe as calculated by SCF/CI (circles) (Ref. 22), and by the HFD (solid line) (Ref. 24) methods.

which is shallower than the CaHe surface calculated by Czuchaj *et al.* ( $\epsilon=2.85\text{ cm}^{-1}$ ,  $r_e=7.4\text{ \AA}$ ),<sup>22</sup> also shown in Fig. 5. The fact that this SCF/CI surface is deeper than the HFD surface and has a *larger*  $r_{\min}$  value is an indication that the two  $(X)1^1\Sigma$  surfaces differ at the HF-SCF level. Differences coming from treatment of electron correlations would typically lead to the deeper potential having the *smaller*  $r_{\min}$  value, as seen for the MgHe case above. One can trace the difference between these two surfaces to the fact that Czuchaj and co-workers did not correct their HF-SCF energy for basis set superposition errors.<sup>38</sup> This hypothesis is supported by the fact that the minimum reported by Czuchaj *et al.* is within an angstrom of the position<sup>39</sup> of the “false minimum” originally obtained in our HF-SCF energy before BSSE correction. The CaHe  $1^2\Sigma$  surface of Kleinekathöfer<sup>23</sup> (labeled ATT in the table) is rather deep ( $10.3\text{ cm}^{-1}$ ) with an  $r_{\min}$  position at  $5.1\text{ \AA}$ .

The solvation parameter  $\lambda$  equals 2.1 for the *ab initio* potential (indicating a slight preference for solvation) and 5.5 for the ATT potential (indicating a strong preference for solvation). Only the HFD potential ( $\lambda=1.4$ ), when combined with the Ancilotto model, correctly predicts a surface location for the Ca on He droplets. We note that the HFD potential ansatz is also the only one (of the three which have been used on both Mg and Ca) to predict a  $\lambda$  value for Ca *smaller* than that for Mg. This means that, if the error in the potential calculations are assumed to vary constantly from system to system and/or if the critical value of  $\lambda$  is shifted, only the HFD potential has in it the capability of correctly predicting the behavior of *both* Mg and Ca.

We had hoped that the present measurements would provide a sensitive test of the Ancilotto model. However, given the wide range of  $\lambda$  values predicted for both Mg and Ca with He, such a sharp comparison is not possible at this time. We hope that the present experimental results will motivate renewed attention to these potential surfaces using the most accurate *ab initio* methods. In view of the above it is tempt-

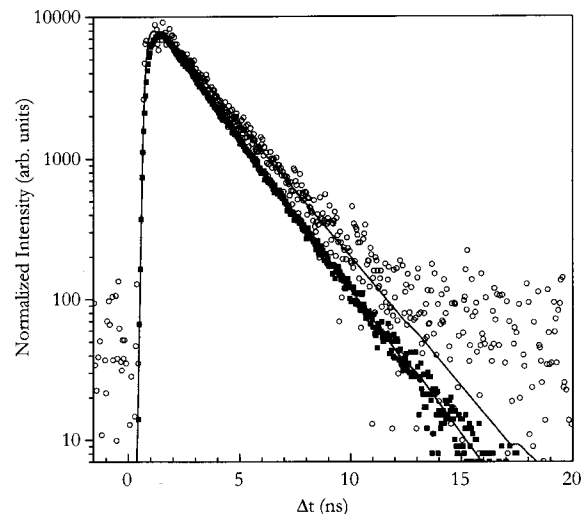


FIG. 6. Log plot of the time evolution of gas-phase (filled squares) and droplet-solvated (open circles) Mg atoms upon  $3^1P_1^0 \leftarrow 3^1S_0$  excitation. The droplet-solvated data are normalized to the gas-phase data for visual comparison. The solid lines are the best fits to the data.

ing to use the Ancilotto criterion as a guide for making educated guesses about the interatomic potentials instead of following the reverse path.

## V. TIME-RESOLVED SPECTRA AND THE LIFETIME OF Mg $3^1P_1^0 \rightarrow 3^1S_0$ EMISSION

Time-correlated single photon counting has been employed in order to temporally disperse the fluorescence emitted upon  $1^1P_1^0 \leftarrow 1^1S_0$  excitation of Mg atoms solvated in He droplets. Figure 6 shows the time evolution of Mg atomic fluorescence both in the gas phase and solvated in He droplets. The count rates measured for these experiments are well below the threshold ( $\sim 30\,000$  counts/s) at which “pile up” error in the TAC becomes a concern.<sup>17</sup> The gas-phase and the droplet-solvated Mg spectra are well fit by a model employing a single exponential rise and a single exponential fall (see Fig. 6). The iterative convolution process used in generating best fits to the time-resolved spectra has been described in detail previously.<sup>16</sup> Here we confine ourselves only to the results. We have found that the fall time (i.e., lifetime) of  $2.05 \pm 0.05$  ns obtained from the emission from the  $3^1P_1^0$  state of gas-phase Mg agrees well with the literature value ( $1.99 \pm 0.08$  ns),<sup>40</sup> while the rise time fit to these data is instrument-limited (i.e.,  $\leq 50$  ps). In the case of the Mg atom in the droplet, the decay lifetime is found to be  $2.39 \pm 0.05$  ns, almost 20% longer than the gas-phase value.

It is well known that the rate of spontaneous emission scales with the cube of the emission frequency, and that many atoms in liquid He have a red-shifted emission.<sup>41</sup> While our Mg signals were too faint to allow for wavelength-dispersed emission, the excellent agreement of our measured excitation profile with that observed previously by Moriwaki and Morita<sup>20</sup> (see Fig. 3) for Mg in bulk He suggests that the emission red shift should be similar in both experiments, i.e.,  $3.2 \pm 0.2$  nm. This accounts for only a 3.5% increase in the emission lifetime compared to the gas phase value.

Assuming that the transition moment and frequency remain the same, the emission lifetime is *shortened* by a factor of the inverse square of the index of refraction of the medium in which the radiator is found itself.<sup>42</sup> This effect, however, arises primarily from the increased photon density of states at a given emission frequency, and does not apply to the present experiment, where the cluster size is much smaller than the wavelength of the emitted radiation.

Penner *et al.* have previously considered the effect of a rare gas cluster environment on the emission lifetime of imbedded molecules.<sup>43</sup> They assume that the dielectric response of the solvent will result in an induced transition dipole that will interfere with that of the chromophore. In the case of a cluster which is small compared to the wavelength, propagation effects can be neglected and electrostatics can be used to estimate the net induced moment, and thus the net “dielectric screening.” For a dipole in a continuum dielectric sphere with relative dielectric constant  $\epsilon_r$ , they demonstrated that the net dipole is reduced by a factor<sup>44</sup> of  $(3/(2 + \epsilon_r))$ , independent of the position or orientation of the dipole inside the sphere. If we estimate  $\epsilon_r$  for a He nanodroplet by the value for bulk He (1.056), we predict a lifetime lengthening of 4%. The Penner *et al.* model, however, treats the dielectric as a continuum around the dipole.

One can approximately account for the exclusion of the He from around the chromophore by putting an emission point dipole in the center of a sphere without dielectric, itself inside a much larger dielectric sphere. Using the methods employed by Penner *et al.*, we have shown that the net external dipole is changed by a factor of

$$9\epsilon_r / (2\epsilon_r^2 + 5\epsilon_r + 2),$$

which represents a negligible change for  $\epsilon_r - 1 \ll 1$ . All this would seem to imply that the dielectric properties of the He have no effect. So far, however, the model has ignored the solvation structure of the He around the excited Mg atom.

We have used an extension of a second method described by Penner *et al.*,<sup>43</sup> which is to sum over all the dipoles induced in the noble gas atoms by the radiating dipole. This ignores the interaction of the induced dipoles, which for He should introduce only a small error<sup>45</sup> on the order of  $\epsilon_r - 1$ . If the radiating dipole is inside a helium droplet with a spatially-dependent He number density,  $\rho(r)$ , we can write the net induced dipole as the following integral:

$$\mu_{\text{IND}} = \mu \cdot 2\alpha \cdot \int \rho(\mathbf{r}) \cdot P_2(\cos \theta) \cdot r^{-3} dv,$$

where  $r$  is the distance from a point in the droplet to the point dipole,  $\alpha$  is the polarizability volume of He ( $0.206 \text{ \AA}^3$ ), and  $\theta$  is the angle between the chromophore transition dipole and the displacement to a point in the He. This first order calculation clearly shows that an isotropic distribution around the chromophore does not generate a net induced dipole moment.

Density functional theory calculations have been carried out in order to study the He density distribution around the excited Mg atom. These calculations have employed a code for pure liquid helium<sup>46</sup> and for helium with impurity atoms<sup>47-49</sup> in which the dopant is treated as a classical object

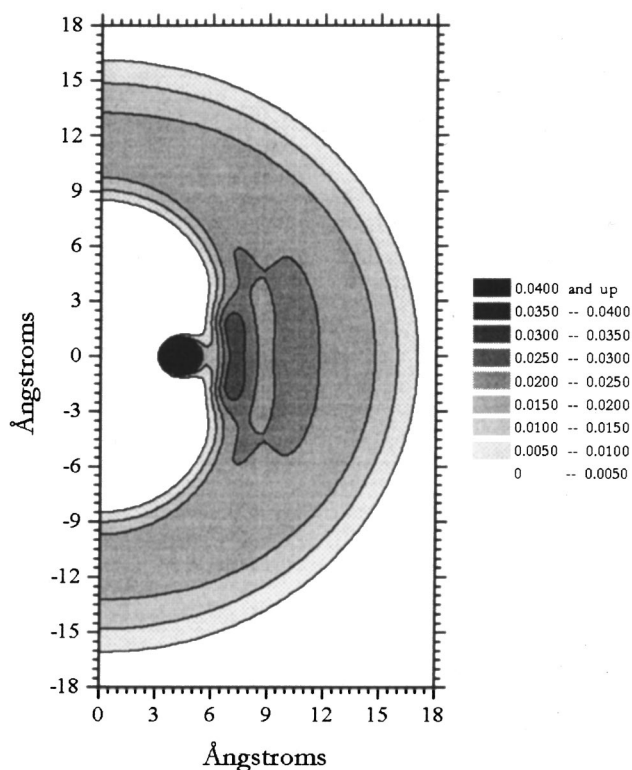


FIG. 7. He density functional contour plot in which a ground state Mg atom is constrained to be in the center (i.e., at 0,0) of a 300-atom helium droplet.

(i.e., devoid of zero point energy) in a quantum liquid. In these studies, the solvation energy of the guest atom inside a  $\text{He}_n$  droplet ( $n = 300-1000$ ) is calculated by comparison with the energy of the same droplet without the solute atom. The dopant atom is treated as an external potential,  $V(r, \theta)$ , around which the helium density is allowed to adjust based upon minimization of the total energy of the system. The He-Mg\* potential is written as  $V(r, \theta) = \cos^2 \theta \cdot V_{\Sigma}(r) + \sin^2 \theta \cdot V_{\Pi}(r)$ , where  $V_{\Sigma}(r)$  and  $V_{\Pi}(r)$  are the He-Mg( $^1P_1^0$ ) pair potentials as given in Ref. 30.

One result from these calculations is the prediction that the He density around the  $^1P_1^0$  state of Mg is strongly anisotropic, with enhanced density perpendicular to the axis of the  $p$  orbital, which is parallel to the transition moment (cf. Fig. 7). Numerical integration of the above expressions predict that the induced moment is 6.2% of the bare Mg transition moment. This leads to a predicted lifetime lengthening of 14%. When combined with the 3.5% effect of the red shift explained above, we arrive at a predicted lifetime lengthening of 17.5%, compared with an experimental value of  $20 \pm 3\%$ .

We consider this agreement to be quite good, especially in light of the simplicity of the model and the uncertainty in the value of the spatially-dependent He density that goes into it. Another approximation is the use of a point dipole for the Mg transition moment, which can be questioned since the size of the  $p$  orbital involved in the transition is of similar spatial extent to the closest Mg-He distances.

An interesting fact that we wish to highlight is that the emission of the solvated Mg is well fit to a single exponential decay with a lifetime value longer than the gas phase value.

This demonstrates that the majority of the Mg atoms stay inside the nanodroplet following excitation. The strong blue shift of the absorption,  $460 \pm 60 \text{ cm}^{-1}$ , argues that the energetics would favor pushing the electronically-excited atom out of the cluster (while likely holding on to its "belt" of He). This event simply does not occur with significant probability during the radiative lifetime. The Mg radiative lifetime is longer than the thermal transit time ( $\sim 0.3 \text{ ns}$ ) of the atom across the nanodroplet, and this points toward a possible barrier to ejection of the excited atom from the cluster despite the high exothermicity of that reaction ( $\sim 21 \text{ K}$ ).

The metastability of electronically-excited Mg inside the cluster contrasts the results of recent measurements by Federmann *et al.*<sup>50</sup> on the dynamics of Ag following electronic excitation. They found that a single 10 ns laser pulse could excite the Ag atom inside the helium droplet ( $5P_{3/2} \leftarrow 5S_{1/2}$ ) and then excite the ( $nS, nD \leftarrow 5P_{1/2}, 20 < n < 60$ ) Rydberg transitions of the free Ag atom.

The reason for the differences in dynamics of electronically-excited Mg and Ag atoms is not apparent. It could be that the fine structure relaxation of the excited Ag atom, which is exothermic by  $920 \text{ cm}^{-1}$ , provides one possibly important difference. In addition, we would like to point out that the methods of Federmann *et al.* strongly favor the detection of the final Rydberg state, and thus it is possible that they are detecting a minor fraction of the total population.

## VI. CONCLUSIONS

The combination of a low vapor pressure metal oven and ultraviolet laser light have provided the opportunity to probe the interaction of Mg atoms with helium nanodroplets. The excitation spectra of Mg evidence the same doubly-peaked structure that has been seen in the case of electronically excited alkali atoms in bulk liquid helium and in the case of Al atoms in helium nanodroplets. Based upon the modeling of alkali data, it is reasonable to conclude that our doubly-peaked profile is due to a quadrupole-induced distortion of the cavity in which the solute atom resides. In the case of the  $3^1P_1^0 \leftarrow 3^1S_0$  transition of Mg solvated in He droplets, the experimental structure and its relative position from the gas-phase transition energy closely correspond with the results of studies conducted in the bulk, demonstrating solvation.

As discussed above, it is not possible at the present time to test the solvation model of Ancilotto *et al.* at values near the predicted threshold of solvation due to uncertainties in the potential energy surfaces which serve as input to the model. It has been shown that while certain *ab initio* and semiempirical surfaces may generate  $\lambda$  values corroborated by experimental findings for a given case, none of the surfaces studied correctly predict the solvation behavior of both Mg (solvated) and Ca (resident on the surface) picked up by helium nanodroplets. It is hoped that the present study, coupled with previous work on Ca,<sup>8</sup> Sr,<sup>8</sup> and Ba,<sup>9</sup> will serve both as an impetus towards and a check for the generation of high-level *ab initio* alkaline earth-He potential energy surfaces. The ability to predict solvation for such "borderline" species with simple, robust models such as that of Ancilotto

*et al.* will prove to be a pivotal step in the continuing work toward the understanding of interactions of guest atoms with the helium droplet matrix.

In reference to the Ancilotto model itself, one possibility worth considering is that the shape of the potential energy surface used as input is not given consideration by the model. It seems that for cases in which  $\lambda$  does not lie near (say, within 0.5) the solvation threshold of  $\lambda = 1.9$ , the shape of the potential surface need not be taken into account, as the Ancilotto model is predictive outside of this narrow threshold window. However, for  $\lambda$  values which lie close to the solvation threshold, consideration of the shape of the potential energy surface, as well as the well depth and equilibrium internuclear distance, seems warranted.

Another step in the direction of understanding of interactions of guest atoms with the helium droplet matrix has come from our time-resolved Mg spectra, which reveal a  $20 \pm 3\%$  increase in the Mg  $3^1P_1^0$  lifetime from the known (and measured) gas phase value. We have quantitatively modeled this lengthening of the lifetime by considering the effect of the anisotropic arrangement of helium atoms around the Mg dopants (as obtained from our density functional calculations) combined with the predicted change in lifetime due to the emission being red-shifted from the excitation wavelength.

## ACKNOWLEDGMENTS

We would like to acknowledge the assistance of Dr. Elmar Schreiber who has assisted us with the laser system used in these experiments. We also thank Dr. Franco Dalfovo for helpful conversations and for making his density functional code available to us. U. M. gratefully acknowledges a Feodor-Lynen postdoctoral fellowship of the Alexander von Humboldt Foundation. This work was carried out under the AFOSR (HEDM program) Grant No. F-49620-98-1-0045. The Princeton Center for Ultrafast Laser Applications is supported by the New Jersey Commission of Science and Technology.

- <sup>1</sup>J. P. Toennies and A. Vilesov, *Annu. Rev. Phys. Chem.* **49**, 1 (1998).
- <sup>2</sup>B. Whaley, *Int. Rev. Phys. Chem.* **13**, 41 (1994).
- <sup>3</sup>F. Stienkemeier, J. Higgins, C. Callegari, S. I. Kanorsky, W. E. Ernst, and G. Scoles, *Z. Phys. D: At., Mol. Clusters* **38**, 253 (1996).
- <sup>4</sup>J. Higgins, C. Callegari, J. Reho, F. Stienkemeier, W. E. Ernst, K. K. Lehmann, M. Gurtowski, and G. Scoles, *Science* **273**, 629 (1996).
- <sup>5</sup>J. Higgins, W. E. Ernst, C. Callegari, J. Reho, K. K. Lehmann, and G. Scoles, *Phys. Rev. Lett.* **77**, 4532 (1996).
- <sup>6</sup>F. Ancilotto, E. Cheng, M. W. Cole, and F. Toigo, *Z. Phys. B: Condens. Matter* **98**, 323 (1995).
- <sup>7</sup>P. B. Lerner, M. W. Cole, and E. Cheng, *J. Low Temp. Phys.* **100**, 501 (1995).
- <sup>8</sup>F. Stienkemeier, F. Meier, and H. O. Lutz, *J. Chem. Phys.* **107**, 10816 (1997).
- <sup>9</sup>F. Stienkemeier, F. Meier, and H. O. Lutz, *Eur. Phys. J. D* **9**, 1 (1999).
- <sup>10</sup>A. Bartelt, J. D. Close, F. Federmann, K. Hoffmann, N. Quaas, and J. P. Toennies, *Z. Phys. D: At., Mol. Clusters* **39**, 1 (1997).
- <sup>11</sup>A. Bartelt, J. D. Close, F. Federmann, N. Quaas, and J. P. Toennies, *Phys. Rev. Lett.* **77**, 3525 (1996).
- <sup>12</sup>F. Ancilotto, P. B. Lerner, and M. W. Cole, *J. Low Temp. Phys.* **101**, 1123 (1995).
- <sup>13</sup>As reported in Table III of E. Cheng, M. W. Cole, W. F. Saam, and J. Treiner, *Phys. Rev. B* **48**, 18214 (1993).

- <sup>14</sup>Based on the potential surface of Z. J. Jakubek and M. Takami, Chem. Phys. Lett. **265**, 653 (1997).
- <sup>15</sup>J. Reho, U. Merker, M. R. Radcliff, K. K. Lehmann, and G. Scoles, J. Phys. Chem. (to be published).
- <sup>16</sup>J. Reho, C. Callegari, J. Higgins, W. E. Ernst, K. K. Lehmann, and G. Scoles, Faraday Discuss. **108**, 161 (1997).
- <sup>17</sup>D. V. O'Connor and D. Phillips, *Time-Correlated Single Photon Counting* (Academic, London, 1984).
- <sup>18</sup>G. Harrison, *Wavelength Tables with Intensities in Arc, Spark, or Discharge Tube* (MIT Press, Cambridge, MA, 1969).
- <sup>19</sup>W. C. Martin and R. Zalubas, J. Phys. Chem. Ref. Data **9**, 1 (1980).
- <sup>20</sup>Y. Moriwaki and N. Morita, Eur. Phys. J. D **5**, 53 (1999).
- <sup>21</sup>T. Kinoshita, K. Fukuda, and T. Yabuzaki, Phys. Rev. B **54**, 6600 (1996).
- <sup>22</sup>E. Czuchaj, F. Rebenrost, J. Stoll, and H. Preuss, Chem. Phys. Lett. **182**, 191 (1991).
- <sup>23</sup>U. Kleinekathöfer (private communication).
- <sup>24</sup>C. Douketis, G. Scoles, S. Marchetti, M. Zen, and A. Thakkar, J. Chem. Phys. **76**, 3057 (1982).
- <sup>25</sup>G. Scoles *et al.* (unpublished results).
- <sup>26</sup>J. M. Standard and P. R. Certain, J. Chem. Phys. **83**, 3002 (1985).
- <sup>27</sup>GAUSSIAN 94, Revision C.3. M. J. Frisch, G. W. Trucks, H. B. Schlegel, P. M. W. Gill, B. G. Johnson, M. A. Robb, J. R. Cheeseman, T. Keith, G. A. Petersson, J. A. Montgomery, K. Raghavachari, M. A. Allaham, V. G. Zakrzewski, J. V. Ortiz, J. B. Foresman, J. Cioslowski, B. B. Stefanov, A. Nanayakkara, M. Challacobe, E. S. Replogle, R. Gomperts, R. L. Martin, D. J. Fox, J. S. Binkley, D. J. Defrees, J. Baker, J. P. Stewart, M. Head-Gordon, C. Gonzalez, and J. A. Pople, Gaussian, Inc., Pittsburgh, Pennsylvania, 1995.
- <sup>28</sup>D. J. Funk, W. H. Breckenridge, J. Simon, and G. Chatasiński, J. Chem. Phys. **91**, 1114 (1989).
- <sup>29</sup>E. Czuchaj, H. Stoll, and H. Preuss, J. Phys. B **20**, 1487 (1987).
- <sup>30</sup>Q. Hui, Ph.D. thesis, Graduate School of Science and Engineering, Saitama University, 1997.
- <sup>31</sup>S. Huzinaga, M. Klobakowski, and H. Tatewaki, Can. J. Chem. **63**, 1812 (1985).
- <sup>32</sup>F. B. van Duijneveldt, IBM Research Report No. RJ 945, #16437, 1971.
- <sup>33</sup>D. E. Woon and T. H. Dunning, Jr., J. Chem. Phys. **100**, 2975 (1994).
- <sup>34</sup>R. Krishnan, J. S. Binkley, R. Seeger, and J. A. Pople, J. Chem. Phys. **72**, 650 (1980).
- <sup>35</sup>A. D. McLean and G. S. Chandler, J. Chem. Phys. **72**, 5639 (1980).
- <sup>36</sup>K. T. Tang and J. P. Toennies, J. Chem. Phys. **80**, 3726 (1984).
- <sup>37</sup>J.-P. Blaudeau, M. P. McGrath, L. A. Curtiss, and L. Radom, J. Chem. Phys. **107**, 5016 (1997).
- <sup>38</sup>E. Czuchaj (private communication).
- <sup>39</sup>The position of this "false minimum" is itself basis set-dependent, and as Czuchaj *et al.* have not employed the same basis in their SCF calculation, there is no need for the positioning to exactly agree in order to make the claim stated in the text.
- <sup>40</sup>A. Lurio, Phys. Rev. **136**, 376 (1964).
- <sup>41</sup>J. Reho, J. Higgins, C. Callegari, K. K. Lehmann, and G. Scoles, J. Chem. Phys. (submitted for publication).
- <sup>42</sup>S. Hirayama and D. Phillips, J. Photochem. **12**, 139–145 (1980).
- <sup>43</sup>A. Penner, A. Amirav, J. Jortner, and A. Nitzan, J. Chem. Phys. **93**, 147 (1990).
- <sup>44</sup>This is different from the factor of  $1/\epsilon_r$ , one might expect because one must include an induced dipole created on the surface of the cluster.
- <sup>45</sup>K. K. Lehmann and J. A. Northby, Mol. Phys. **97**, 639 (1999).
- <sup>46</sup>M. Casas, F. Dalfovo, A. Lastrì, L. Serra, and S. Stringari, Z. Phys. D: At., Mol. Clusters **35**, 67 (1995).
- <sup>47</sup>J. Dupont-Roc, M. Himbert, N. Parloff, and J. Treiner, J. Low Temp. Phys. **81**, 31 (1990).
- <sup>48</sup>F. Dalfovo, Z. Phys. D: At., Mol. Clusters **29**, 61 (1994).
- <sup>49</sup>K. K. Lehmann, Mol. Phys. **97**, 645 (1999).
- <sup>50</sup>F. Federmann, K. Hoffmann, N. Quaas, and J. D. Close, Phys. Rev. Lett. **83**, 2548 (1999).